Thermal performance and design parameters investigation of a novel cavity receiver unit for parabolic trough concentrator

Khaled Mohamad[a,c,*], P. Ferrer[a,b]

[a]*School of Physics, Materials for Energy Research Group, University of the Witwatersrand, Johannesburg, 2001, South Africa.*

[b]*School of Physics, Mandelstam institute for Theoretical Physics, University of the Witwatersrand, Johannesburg, 2001, South Africa.*

[C]*School of Engineering, International Alatoo University, Bishkek, Kyrgyzstan.*

In this paper, we discuss an improved concept of for a cavity receiver unit for Solar Parabolic Trough Collectors (PTC) with the application of hot mirror coating (HMC) on a cavity aperture. This design aims to lessen radiant energy losses while operating at higher temperature by incorporating a variety of optically active layers. We present the theoretical background, which we derived in previous work, and the resulting implementation in a simulation code. We next discuss the layout and results of an experiment, which allowed us to make contact with the simulation with minor adjustments It was seen that the correspondence between the experiment and simulation results was encouragingly close (Chi squared $p > 0.8$ and $p > 0.95$), and we proceeded to investigate simulations of different receiver designs. Simulated outcomes for the temperature of the heat transfer fluid, temperature maps and efficiencies are presented. Our proposal indicates temperature related benefits when compared to other popular designs in terms of the heat transfer fluid temperature and the efficiency.

Keywords: Parabolic trough collector; Receiver unit; Heat transfer fluid; Hot mirror coating; Cavity absorber.

1. Introduction

PTC technology is one of the earliest and most widely accepted designs for harnessing solar energy for electrical and thermal use. It promises to be cost-effective with a possibility to be hybridized with fossil fuels or other renewable power plants. Furthermore, it ensures the best land use among CSP technologies [1].

At the time of writing, there are 86 operational commercial PTC power plants worldwide, and 16 more under construction or development, mostly in Spain and the United States [2].

In a PTC layout, radiation from a source is focused along a pipe shaped receiver unit. The receiver temperature rises, and so does the Heat Transfer Fluid (HTF) contained within. The heated HTF can be used in a variety of thermal applications. The layout of the receiver unit directly influences the efficiency of the entire system [3]. It must be designed in a way to reduce thermal losses.

Conventionally, the receiver–contains an absorber pipe enclosed by a glass tube. The region between is kept at low pressures to reduce convective heat losses. Conduction heat losses are reduced by minimizing the thermal contacts between the glass cover and the absorber pipe.

Increasing the outlet HTF temperature improves the overall efficiency of the PTC power plant and reduces the Levelized Cost of energy and the combined thermal storage. For example, thermal storage quantity can be reduced to one third, if the HTF temperature rises from 350 °C to 600 °C [4]. However, some complications start to appear at a high temperature (> 300 °C) such as thermal stress across the receiver and heat losses due to thermal emission.

The leading heat loss mechanism due to the receiver at high temperatures is via thermal emission (IR). This loss can be greatly reduced by coating the outer surface of the receiver pipe with a selective material, which is a good absorber for light in visible solar spectral region but emits weakly in the IR. Selective coatings and improving their properties is an active field of research [5][6][7]. Since the selective coatings are placed on absorber pipe of the receiver, the receivers' operational temperature is largely restricted by the thermal breakdown temperature of the coatings, although the thermal constraints of the HTF are also important, they are not considered in this work.

An alternative to the selective coating of the absorber pipe is application of a dielectric transparent (in visible) material inside the glass cover which reflects efficiently in the infrared. This type of coating is called a "hot mirror coating" (or "heat mirror coating") [8][9] [10] [11]. The advantage of such an application is due to the glass cover being typically much cooler than the absorber pipe, and hence the absorber pipe's operating temperature can be raised until the glass cover temperature reaches the thermal breakdown limit of the hot mirror coating.

An alternative design to the above-mentioned evacuated receiver is the cavity receiver, which consists of an opaque sleeve surrounding the absorber pipe and usually replaces the glass cover of conventional units. It has an aperture opening allowing solar radiation to enter. A detailed study [12] found that the cavity geometry and the aperture opening of the cavity has a substantial effect on the optical efficiency and the solar flux distribution inside the receiver. Cavity thermal losses are effected by surface emissivity, mass flow rate, HTF temperature, and wind velocity. The cavity helps to reduce the temperature gradient and thermal stresses due to the effect of the multiple reflections in the case of a mirror cavity. In a cylindrical cavity receiver, if there is no vacuum in the annulus, the convection and conduction heat loss can be minimized by selecting the optimum annulus dimension between the absorber pipe and the cavity envelope, which largely depends on the diameters of the receiver components[4][13]. The hot mirror application on the glass cover can further diminish the IR losses and thermal stresses. The cavity geometry with an aperture hot mirror coating allows for larger retention of thermal radiation in the receiver [14][15][11][16]. A triangular cavity receiver has the highest optical efficiency among the non-cylindrical cavity receivers followed by the elliptical cavity with flat plate reflector [17][18][19]. V-shape receiver with rectangular fins showed a better heat performance with higher outlet HTF temperature than using the absorber without fins. Further, the V- shape receiver indicated a potentially large improvement in future work [20][21]. The efficiency of the trapezoidal cavity receiver for linear concentrating solar collector is comparable to the efficiency of the metal glass evacuated tube if the optimized parameters are selected [22]. All the above projects involved cavities that were not evacuated. A comprehensive review on the subject of the cavity system designs is given by [12].

We present a design of a PTC receiver unit that combines a cavity design and hot mirror coating in a new way. A highly reflective (in visible and IR spectral regions) cavity surrounds the absorber pipe, which has an aperture with a hot mirror coated glass cover as a solar radiation inlet. The cavity is evacuated. The cavity walls reflectivity and the aperture with a hot mirror coating allow much larger containment of thermal radiation inside the receiver unit. The design was analyzed numerically and studied experimentally. Some added features of the base theory for the design are mentioned and their implementation described in a simulation code. An experimental setup of the cavity receiver unit was constructed and data collected. The experimental results were compared to our simulation results with good correspondence. Encouraged by this positive result, we proceeded to investigate further performance simulations, such as receiver and HTF temperature profiles and their related efficiencies.

2. A mathematical description for a cavity receiver with hot mirror aperture

2.1. The cavity receiver design description

A metallic cavity sleeve with a windowed aperture surrounds the inner absorber pipe, see Figure 1. The cavity material consists of a IR reflective mirror, such as aluminum, on the inner surface, while the inside of the borosilicate glass aperture is coated with a HMC. A vacuum between the cavity surface and absorber pipe reduces convective losses. The polished aluminum surface inside the cavity returns IR radiation onto the absorber pipe via reflection very effectively.

We discuss the model of the radiation behavior inside the receiver in the following sections.

2.2. Descriptions of the heat fluxes

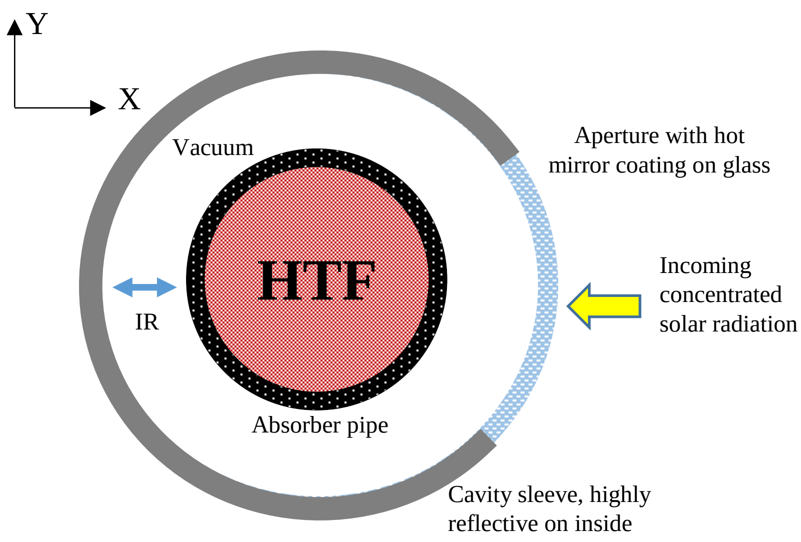

Figure 1: Schematic of the receiver cavity. A glass aperture with a HMC and a cavity sleeve with a highly reflective surface prevents IR radiation from escaping.

Under the steady-state condition, the heat flux of the absorber pipe and the outer surface can be described as in Figure 1. Concentrated solar radiation (from a solar parabolic trough mirror) passes into the cavity aperture is mostly absorbed by the absorber pipe, which increases in temperature. This leads to emission of IR radiation from the absorber pipe to the cavity walls which is mostly reflected back, as well as to the outside since the cavity walls will invariably absorb some radiation and heat up. Heat is transferred via convection between the outer cavity wall and the surrounding, and between the inside absorber pipe and the fluid (HTF) within, but is neglected in the evacuated region. Radiation is exchanged with the environment. Conduction through structural support fixtures was neglected.

The receiver was discretized into control volumes (CV) to take into account the non-uniform solar influx ~~into account~~. The cavity wall and the absorber pipe were segmented into control volumes along the circumference. The HTF is similarly discretized but in the z-axis direction (longitudinally) only, see Figure 2. Under steady state conditions, an energy conservation equation is written as

$$\left(\sum \dot{q}_{COND} + \sum \dot{q}_{RAD} + \sum \dot{q}_{CONV} + \sum \dot{q}_{sol}\right)_j = 0 \tag{1}$$

Eq. (1) is enforced on ~~every~~ each CV on both the glass cover and the absorber pipe, where $\dot{q}_{COND}$, $\dot{q}_{CONV}$, $\dot{q}_{RAD}$, and $\dot{q}_{sol}$ are conduction, convection, radiation and solar radiation heat transfers respectively.

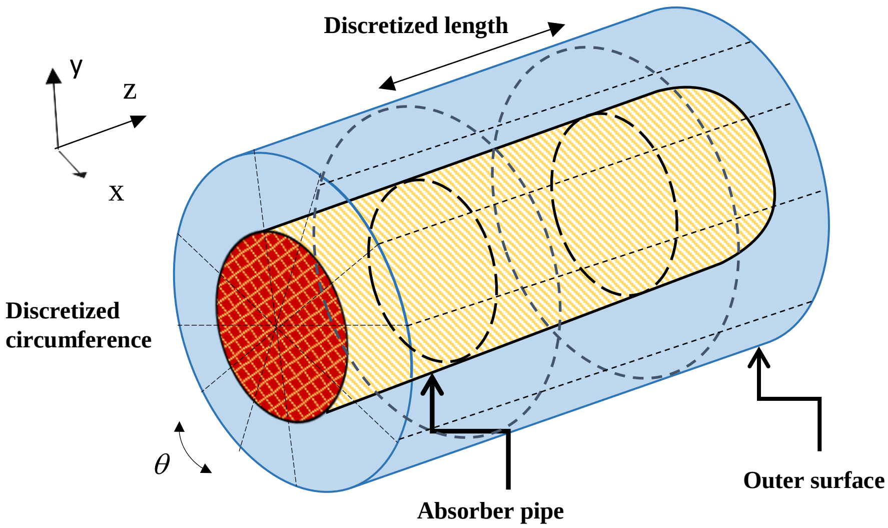

Figure 2: The discretization of the receiver unit.

A set of non-linear equations for the temperature can thus be obtained for every control volume, which can be linearized to give

$$a_m T_m = a_{m+1} T_{m+1} + a_{m-1} T_{m-1} + b_m, \tag{2}$$

where T_m, a_m, and b_m are the temperature, the discretization coefficient, and the discretization source term of the control volume "m" respectively. The terms with index $m+1$ and $m-1$ are for the neighbouring control volumes. The terms of Eq. (2) are defined for absorber pipe and outer (cavity) surface control volumes. These results were derived in [23][10][24], and we only quote the central results here.

For the absorber pipe:

$$a_m = k_A \frac{2\times\Delta S_A \Delta L}{\left(r_A+\frac{\Delta S_A}{2}\right)\theta_A} + h_f[r_A\theta_A\Delta L] + 4\varepsilon_A\sigma dA_A \times \left(1+ \rho_A\, \rho_{HM_{2m}} F^{HM,A}_{2m,m} \left(\sum\nolimits_k F^{A,HM}_{mk} - F^{A,HM}_{m,2m}\right)\right) \times {T^{A}_{ml}}^{3} - (1-\rho_A)\times(4\varepsilon_A\sigma dA_A)\times\left(\rho_{HM_{2m}} F^{HM,A}_{2m,m} + \rho_A\, {\rho_{HM_{2m}}}^{2}\, {F^{HM,A}_{2m,m}}^{2}\right) {T^{A}_{ml}}^{3}, \tag{3}$$

$$b_m = \alpha_{viis,A}\,\tau_{vis,HM}\,dA_A\left(\dot{Q}_{A,sol}\right)_m + h_f dA_A\,T_l^f + 3\varepsilon_A\sigma dA_A \times \left(1 + \rho_A\,\rho_{HM_{2m}}F_{2m,m}^{HM,A}\left(\sum_k F_{mk}^{A,HM} - F_{m,2m}^{A,HM}\right)\right) \times {T_{ml}^{A}}^{4} - (1-\rho_A)\times(3\varepsilon_A\sigma dA_A)\times\left(\rho_{HM_{2m}}F_{2m,m}^{HM,A} + \rho_A\,{\rho_{HM_{2m}}}^{2}\,{F_{2m,m}^{HM,A}}^{2}\right){T_{ml}^{A}}^{4} + (1-\rho_A)\times\left(\left(\dot{Q}_{IR,1ref}\right)_{ml} + \left(\dot{Q}_{IR,2ref}\right)_m\right) + (1-\rho_A)\times\,\varepsilon_{HM}\sigma dA_{HM}\,\sum_k F_{km}^{HM,A}\,{T_{kl}^{HM}}^{4}, \tag{4}$$

$$a_{m+1} = a_{m-1} = \frac{\Delta s_A \Delta L}{\left(r_A + \frac{\Delta s_A}{2}\right)\theta_A}. \tag{5}$$

and for the outer (cavity) surface:

$$a_m = k_{HM}\frac{2\times\Delta s_{HM}\Delta L}{\left(r_{HM} + \frac{\Delta s_{HM}}{2}\right)\theta_{HM}} + h_w dA_{HM,out} + 4\sigma\times\left(\varepsilon_{HM,in}dA_{HM,in} + \varepsilon_{HM,out}dA_{HM,out}\right){T_{ml}^{HM}}^{3}, \tag{6}$$

$$b_m = \alpha_{viis,HM}\,dA_{HM,out}\left(\dot{Q}_{HM,sol}\right)_m + h_w dA_{HM,out}\,T^O + 3\sigma\times\left(\varepsilon_{HM,in}dA_{HM,in} + \varepsilon_{HM,out}dA_{HM,out}\right){T_{ml}^{HM}}^{4} + \varepsilon_{HM,out}\sigma dA_{HM,out}\,T_{sky}^4 + \left(1-\rho_{HM_m}\right)\times\left(\left(\dot{Q}_{IR,1ref,HM}\right)_{ml} + \left(\dot{Q}_{IR,2ref,HM}\right)_{ml}\right) + \left(1-\rho_{HM_m}\right)\times\,\varepsilon_{HM}\sigma dA_{HM,out}\,\sum_k F_{km}^{HM,HM}\,{T_{kl}^{HM}}^{4}, \tag{7}$$

$$a_{m+1} = a_{m-1} = \frac{\Delta s_{HM}\Delta L}{\left(r_{HM} + \frac{\Delta s_{HM}}{2}\right)\theta_{HM}}. \tag{8}$$

where the parameters are defined as follows: $k_{A/HM}$ is the thermal conductivity, $\Delta s_{A/HM}$ is the arc length, ΔL is the length of a control volume, $r_{A/HM}$ is the radius of the surface, $\theta_{A/HM}$ is angle of control volume, h_f is convective heat transfer coefficient for the HTF, dA_1 is the differential area on a surface 1, ε is the surface emissivity, σ is the Stefan-Boltzmann constant, ρ denotes reflectivity and $F_{km}^{HM,A}$ is the view factor from control volume "*k*" in HM to "*m*" in AP. Further, T_{ij}^{A} temperature of control volume (*ij*) on surface A, α and τ are the spectral absorptivity and transmissivity, respectively, Q_{sol}, $Q_{IR,1refl}$ and $Q_{IR,2refl}$ are the solar power, the radiation power of the first and second IR reflected rays respectively and T_o and T_{sky} are the ambient temperatures. The label *A/HM* may refer to either "absorber" or "hot mirror", depending on whether they are situated inside the cavity, or are referring to the cavity wall.

These equations are solved through an iterative process. In this process, the heat transfer fluid (HTF) temperature along the length is computed using energy balance, where a HTF control volume "*l*" is described as:

$$\left(\dot{Q}_{AF,conv}\right)_l = \sum_{m=1}^{N_m} h_f dA_A\left(T_{ml}^A - T_l^F\right) = \dot{m}C_P\left(T_{l+1}^F - T_l^F\right). \tag{9}$$

where C_P and $\dot{m}$ are the HTF specific heat capacity and the mass flow rate respectively. Eq. (9) allows us to find the value of the temperature of the next HTF control volume T_{l+1}^F.

The simulation algorithm of the receiver unit that operates with non-uniform heat flux is summarized in Figure 3. It has the following structure: HTF passes into the absorber pipe with a temperature T_l^F. For all AP and the outer cover control volumes, the initial HTF inlet temperature *T** is guessed. Eq. (2) is iteratively solved for all the control volumes to ~~obtain~~ find a ~~new~~ different temperature estimate *T*, which becomes the subsequent input for *T**. The iterations terminate once a convergence criterion is achieved, which was chosen as $\frac{T^{\mathrm{n}+1}-T^{\mathrm{n}}}{T^{\mathrm{n}}} < 10^{-6}$ (*n* denotes the n^{th} iteration). A knowledge of *T* allows determination of the heat transferred into the HTF using Eq. (9). Th HTF exit temperature is taken as the entry temperature for the subsequent "ring" section, see Figure 2. This process continues for the entire receiver length.

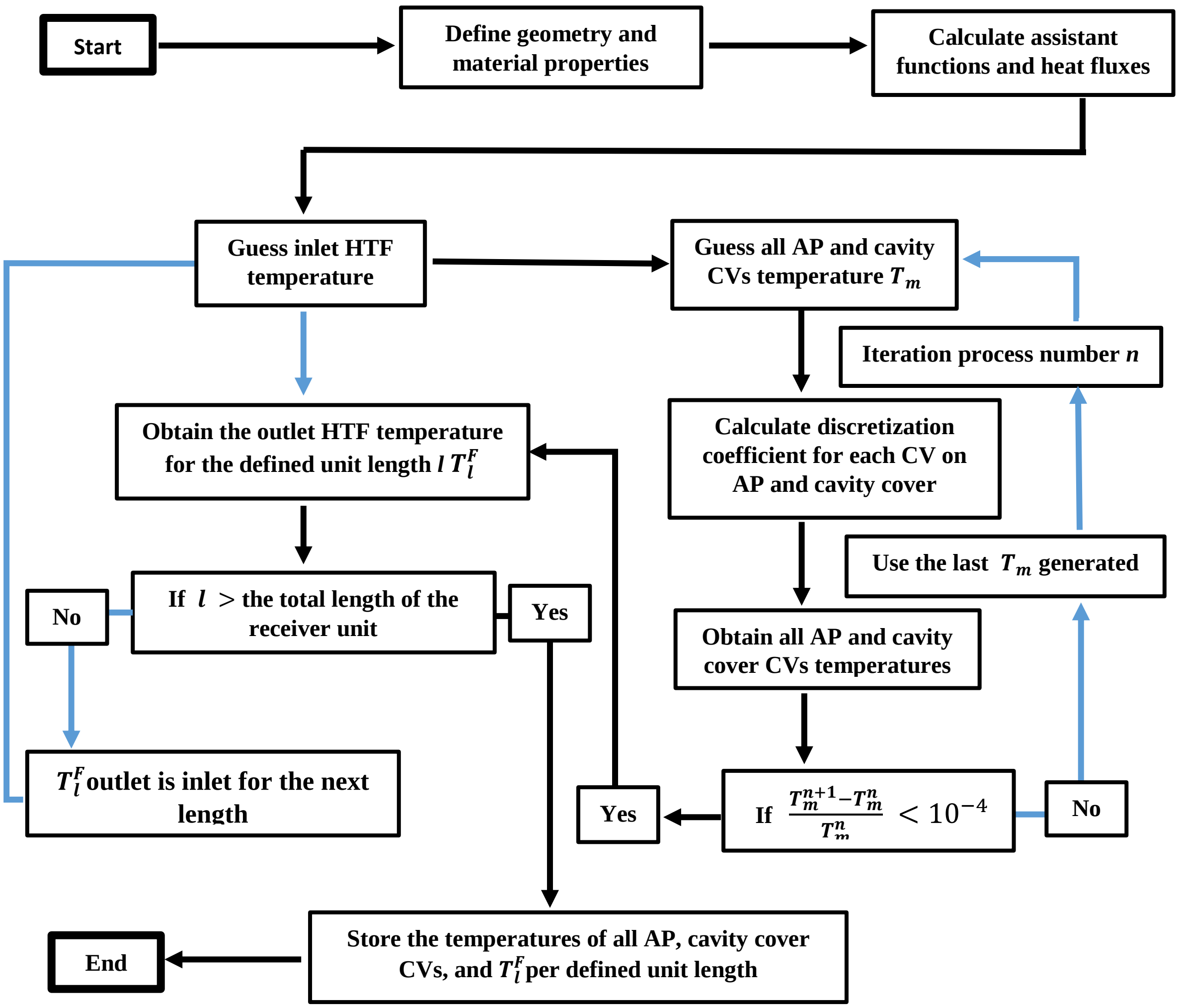

Figure 3: Illustration of the algorithm of the simulation code in case of the receiver that operates with non-uniform heat flux. Black arrows are for the primary processes execution and true conditions and the blue arrows, for the false and iterative conditions.

The convergence tests of the simulation codes were performed to estimate the adequate numbers of control volumes and values for the convergence criterions. Some assumptions were made in the simulation:

- The HTF is incompressible.
- The absorber pipe surface emits and reflects diffusely.
- Hot mirror (HM) and IR reflective mirror (IRM) are secularly reflective in the IR.
- Radiative fluxes are a surface phenomenon.
- Across the boundary surfaces of each successive control volume, the temperature profile is linear.

The simulation has the ability to provide HTF temperature values along the length and the thermal distribution along the circumference of both the outer cover and the absorber pipe. It also describes the energy losses originating from the differing mechanisms along the length. This information can be used to deduce the efficiency of the system.

Thermal efficiency of the receiver unit is heat gain in the fluid divided by the total incident solar energy, which considers all losses [25]. The thermal efficiency for each control volume (CV) is

$$\eta_{CV} = \frac{(\dot{q}_{AF,conv})_j}{(q_{sol})_j}, \tag{10}$$

where q_{sol} the incoming solar flux, and $(\dot{q}_{AF,conv})_j$ is given by Eq.(9). The summed or "integrated" efficiency for *n* control volumes along the system's length is

$$\eta = \frac{\sum_{j=1}^{n}(\dot{q}_{AF,conv})_j}{\sum_{j=1}^{n}(q_{sol})_j}. \tag{11}$$

The thermal energy output from the PTC is converted into electricity in many applications. The overall efficiency "maximum" η_{max} of the PTC plant and the conversion part for electric power generation (turbine) can be estimated using a Carnot Cycle, which is given by

$$\eta_{max} = \frac{\sum_{j=1}^{n}(\dot{q}_{AF,conv})_j}{\sum_{j=1}^{n}(q_{sol})_j} \times \left(1 - \frac{T_{res}}{T_{HTF}}\right), \tag{12}$$

where T_{HTF} and T_{res} are HTF temperatures and ambient temperature (it is the cold reservoir), respectively.

3. Results and discussion

3.1. Simulation and Experiment

We first use the simulation in a way to make contact with experiment

An experiment in line to test the model simulation described above was conducted. A receiver was produced similar to an operational PTC but heated by elements from within.

The unit was used indoors. Its length was 3.9 m at 25 ℃. It was constructed of three steel pipe sections for the outer cover of the cavity receiver, each 1.3 m long with outer/inner diameter of 7.7/6.7 cm. Each section had an opening window along the length with a width of 1.8 cm. Borosilicate glass plates with 3.5 cm width and 0.38 cm thick were affixed on the outer cover aperture window using flame resistance high-temperature silicon.

An absorber pipe with inner and outer diameter of 2.8 cm and 3.2 cm respectively were situated co-centrically inside the receiver unit, see Figure 4 and 5. The connections between the various components were sealed using a heat resistant silicon sealant, which provided contact insulation.The space inside the receiver was evacuated using a rotary vacuum pump (input: 208-230 VAC, 60/50 HZ).

Figure 4: The set-up of the receiver unit in the laboratory.

Three 1.5 kW heating elements inserted along the inner pipe brought the HTF temperature to adjustable values, with the help of a single phase variable transformer variac. The power input was calculated by noting simultaneously current and voltage, with an error of ± 7 W. The total cold resistance of the elements inside the absorber pipe had a value of 11 ± 0.1 Ohm. The absorber pipe also contained fine sand to simulate aspects of a heat transfer fluid by allocating heat evenly to the surface of the absorber pipe.

Nine K-type thermocouples (glass fiber twisted insulation, with measurement range -200 °C to 1350 °C) were attached as shown in Figure 5, to calculate the average temperatures (± 1 °C) and observe heating behavior. This information allowed us to compute the heat loss to the environment.

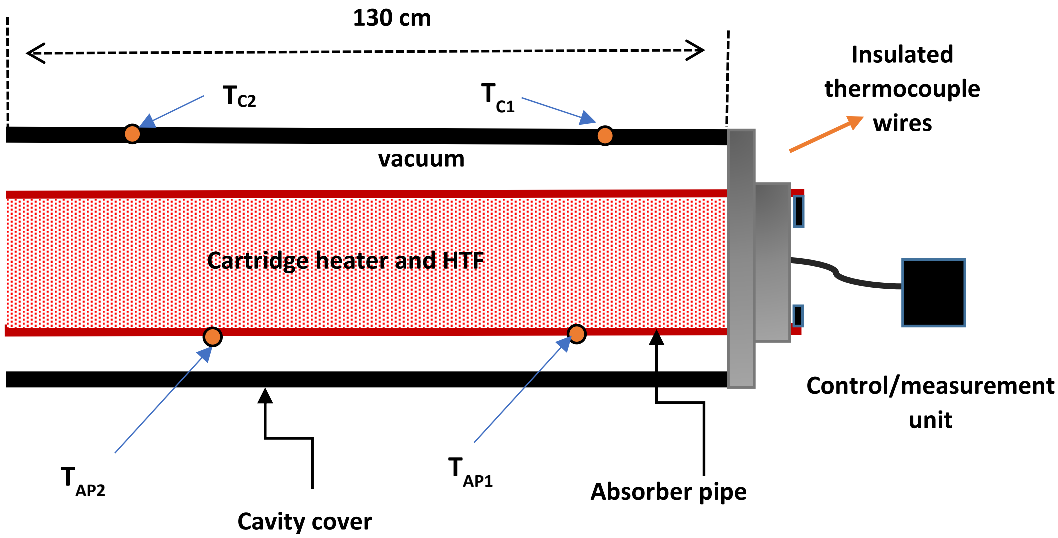

Figure 5: Cross section of one receiver unit. The absorber pipe, cavity cover, thermocouples and heaters (indicated by "T") are shown.

The thermocouple wires were linked to the measurement unit, which controlled the heater power as required (see Figure 4 and 5).

The measurements began by evacuating the units down to < 0.1 mbar (measurement with a vacuum gauge KJL 275i), to quench convective heat transfer between absorber pipe and cavity wall [26]. The variac was adjusted for an initial heating of around 50 W, which was subsequently determined more accurately using the voltage and current measurements (Brymen voltmeter TBM815 (errors on Resistance = 0.1% and V (AC) = 0.5%). The thermocouple temperature readings were logged using an Arduino Mega thermocouple shield (MAX6675)) microcontroller. Thermal equilibrium was typically reached within about three hours. All temperatures were recorded, and the process would repeat with a higher power setting. The experiment terminated at a power input of approximately 2 kW, due to vacuum system temperature concerns.

At thermal equilibrium, the heat loss through the outer cover equated to the electrical power into the system. All heat losses are reported in units of Watts per meter.

3.1.1. Experimental validation: simulation code with uniform heat flux

The theoretical and the numerical model of the thermal interactions is the same as discussed in section 2 except: the heat originates from the absorber pipe outer surface due to the heating element inside which allows us to ignore effects related to the HTF in the calculations. The convection heat transfer term and the incident solar radiation term are removed from the previously derived energy balance equations [11][27][23].

As thermal equilibrium is reached, the outer cover and absorber pipe stabilize at different stagnation temperatures. Moreover, the heat gain and loss of any individual receiver element equals the overall heat generation rate of the heating elements $\dot{E}_{gen}$

$$\dot{q}_{HM,amb} = \dot{q}_{HM,cond} = \dot{q}_{AP,HM} = \dot{q}_{HM,AP} = \dot{E}_{gen}, \tag{13}$$

where $\dot{q}_{HM,cond}$ and $\dot{q}_{HM,amb}$ are the conduction heat transfer through the HM layer and the rate of the heat transfer from the HM cover to the environment, respectively. $\dot{q}_{AP,HM}$ is the heat transfer from AP to HM.

The algorithm schematic is shown in Figure 6, and shares similarities with the simulation discussed above: we start by guessing the temperature of the outer cover control volumes (glass or HM + IRM) with a specified initial temperature T_m^n. It is an iterative solution until the heat loss of the outer cover to the ambient is equal to the heat power generation of the heating elements. By knowing the outer cover temperature, the inner temperature of the outer cover control volumes (CVs) can be calculated through the conduction heat transfer between outer cover widths. At this point, all control volumes of the same surface are in thermal equilibrium, while the temperatures of different surfaces are different. The program iterates an initially guessed T* by solving Eq. (2) for all the control volumes on AP to obtain a next estimate for subsequent T* till the criterion, $\frac{T^{\mathrm{n+1}}-T^{\mathrm{n}}}{T^{\mathrm{n}}} < 10^{-4}$ is achieved.

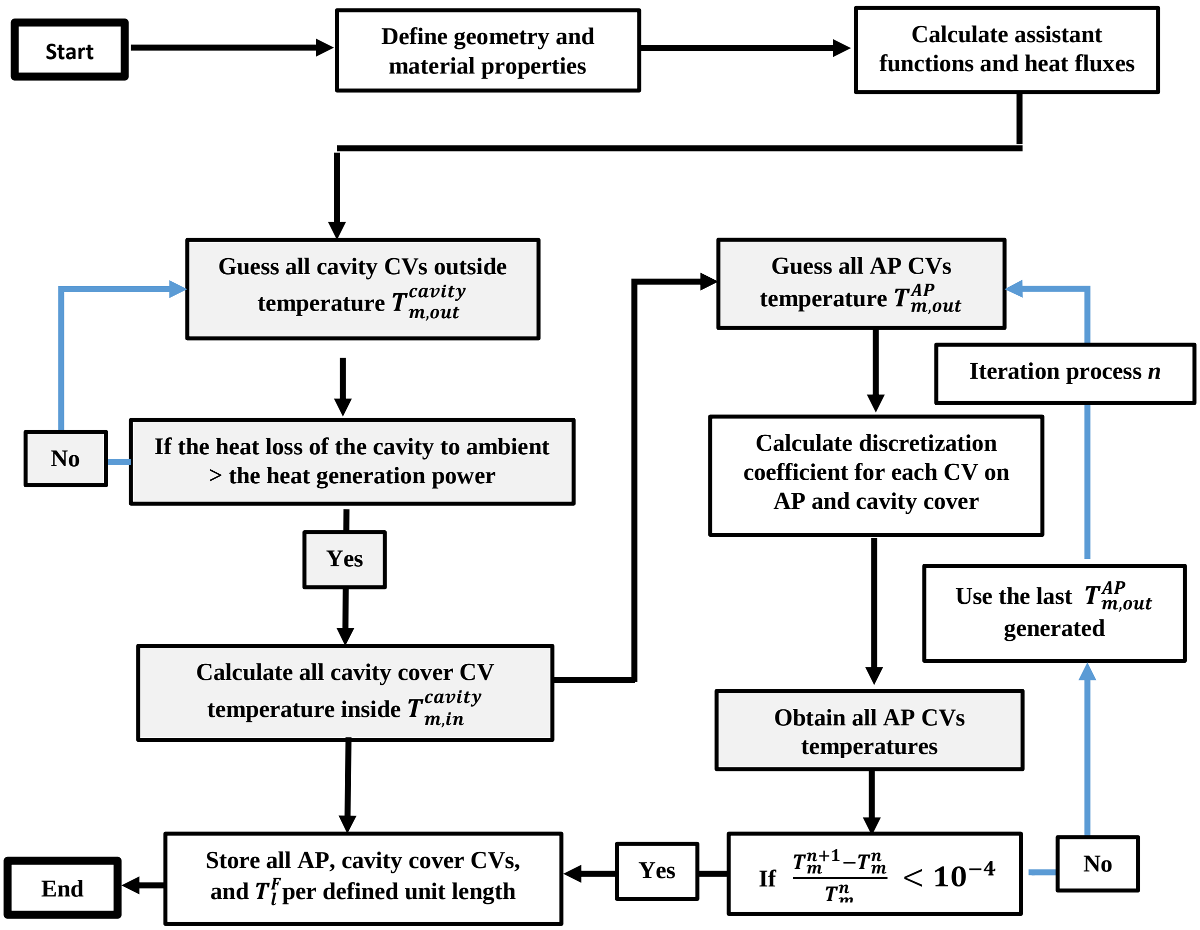

Figure 6: Illustration of the algorithm of the simulation code in case of the receiver unit that operates with uniform heat flux. Black arrows are for the primary processes execution and the true conditions and the blue arrows, for the false and iterative conditions. The colored blocks indicate a difference to the previous algorithm.

The data obtained from the experimental setup was compared to the simulation. The optical parameters of our receiver components are given in Table 1.

Table 1: The absorber pipe and outer cover optical properties [16][28][29].

		Absorber pipe	Borosilicate glass	Hot mirror (ITO)	IR mirror cavity
Visible	**Transmissivity**	0	0.935	0.875	0
	Reflectivity	0.14	0.04	0.10	0.92
Infrared	**Transmissivity**	0	0	0	0
	Reflectivity	0.14	0.14	0.850	0.92

Figure 7 shows the results of the power density (W/m) versus temperatures (Celsius). Experimental results (EXP) and simulation (SIM) results are shown. It is seen from Figure 7 that the results of SIM and EXP for the cover deviate maximally 0.9%, while those of the absorber pipe diverge mostly by 6% at around 500 Celsius. A Chi squared analysis gives p-values greater than 0.95 for the cavity cover and p-value of >0.8 for the absorber pipe, indicating that our description fits the data very well.

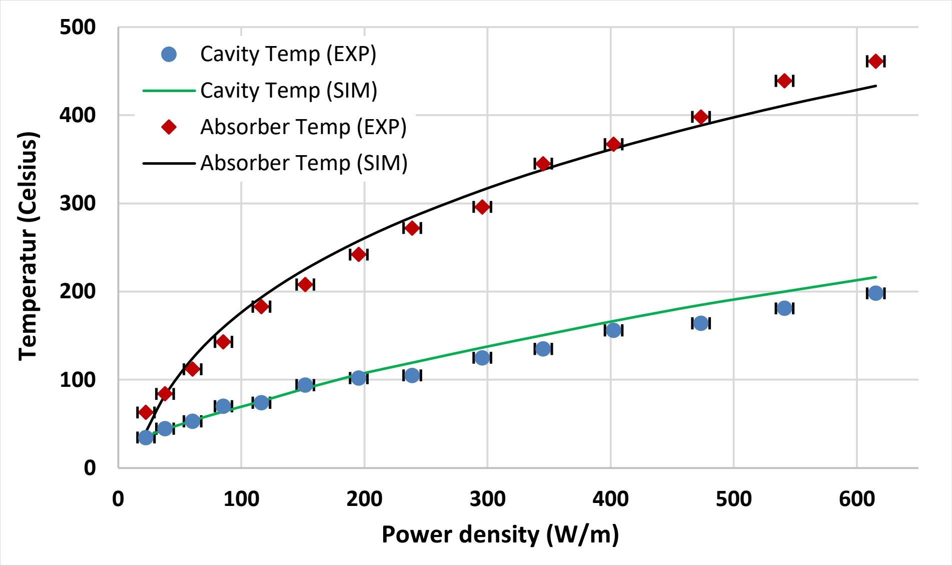

Figure 7: The temperature profile of simulated and experimental results at different heating powers for the cavity receiver.

3.2. The proposed Cavity design results of realistic scenarios

In section 6.2, the simulation codes were shown to be a good description of the experimental results. The original simulation code of figure 3 can next be utilized to study the proposed cavity receiver design with a hot mirror application, as well as alternative receiver designs with different active layer applications. Although this code is slightly different from the experimentally compared code of the previous section, the main elements and theory are identical.

The operating conditions and design parameters used in the following simulation are similar to the condition at SEGS (Solar Electric Generating System) [28]. The parameters are listed in Table 2. However, some optical parameters were modified to fit the cavity requirements, see Table 1.

Table 2: The SEGS LS2 parameters used in the present simulation.

Parameter	***Value***
Collector aperture (a)	5 m

Focal length (f)	1.84 m
Absorber pipe inner diameter	0.066 m
Absorber pipe outer diameter	0.07 m
Absorber pipe emissivity in IR	0.15
Glass tube inner diameter	0.109 m
Glass tube outer diameter	0.115 m
Glass tube emissivity in IR	0.86
Absorber pipe absorptance in visible	0.96
Glass tube transmittance in visible	0.93
Parabola specular reflectance	0.93
Incident angle	0.0
Solar irradiance	933.7 W/m^2
Heat transfer fluid	Molten salt
Mass flow rate	0.68 kg/s
Inlet temperature of Heat transfer fluid	375.35 K
Ambient temperature	294.35 K
Wind speed	2.6 m/ s

3.2.1. Cavity aperture size effects on HTF temperature and efficiency

Solar radiation enters only through the cavity opening. Its size has a noticeable effect, especially at elevated temperatures (>900K). A focal line from a parabolic concentrator has a restricted width due to the angular sun size [30], and the minimum size of the aperture required to be larger than this width for the concentrated solar radiation to be captured by the receiver. Thus, the aperture size was chosen as 48 mm [30] in conjunction with the design parameters of Table 2.

We simulated four different cavity opening sizes, see Figure 8, to estimate the impact on efficiency of this parameter. We used the lengths of 100, 70, 50, and 30 control volumes (which corresponds to the arc lengths of 180 mm, 126 mm, 90 mm, and 54 mm respectively).

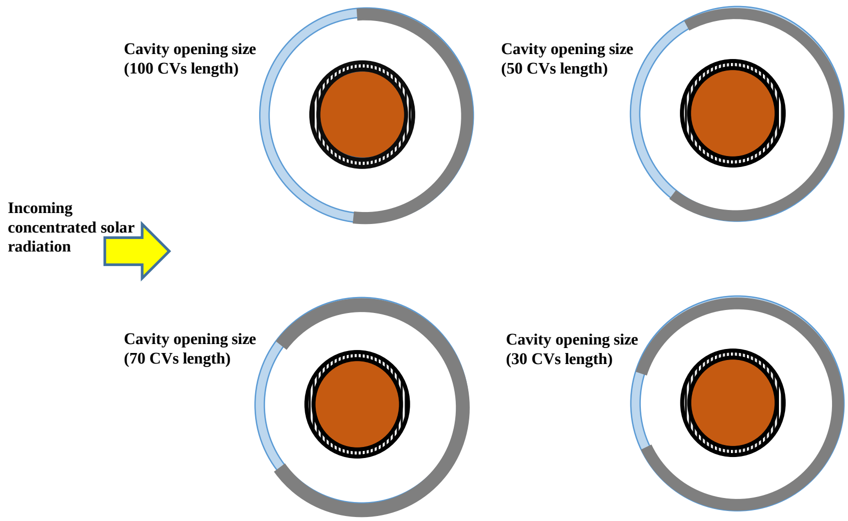

Figure 8: The cavity design cross-section with four cavity opening sizes

Figure 9 displays the temperature of the HTF versus receiver length L(m). Temperature grows approximately linearly and then approaches a stagnation limit, at which the energy gains and losses are equal. The cavity with the lowest opening size reaches the maximum stagnation temperature. Influx of solar radiation is the same for all cases, but losses through IR radiation are diminished by smaller cavity opening size. The maximally attainable HTF temperature rises to ~1300 K at 100 control volume (CVs) and ~1490 K at 30 CVs.

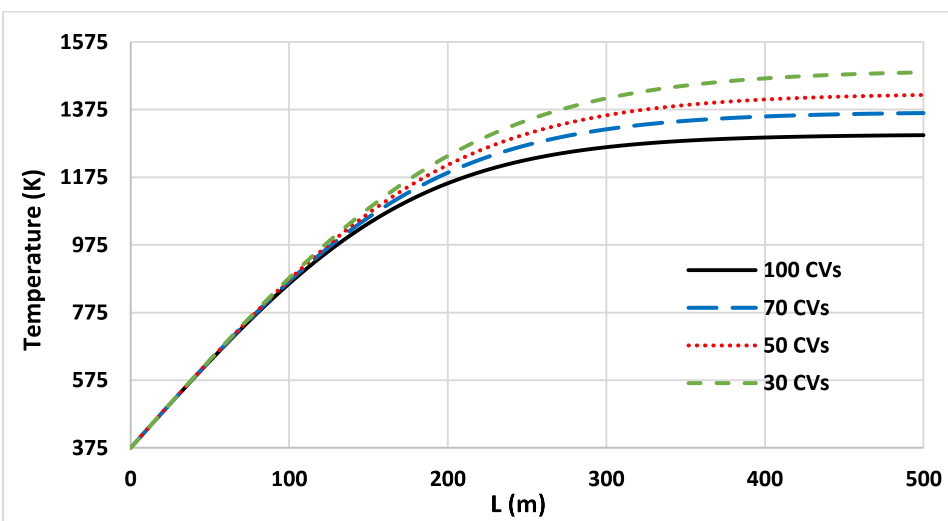

Figure 9: HTF temperature versus the receiver unit length at four cavity opening sizes.

In Figure 10, the integrated efficiency (section 2.2, Eq. (11)) is shown, defined here as the average solar radiation intercepted by the receiver divided by the entire heat transferred into the HTF up to length *L*. It denotes. The solar energy fraction absorbed by the HTF at length *L*.

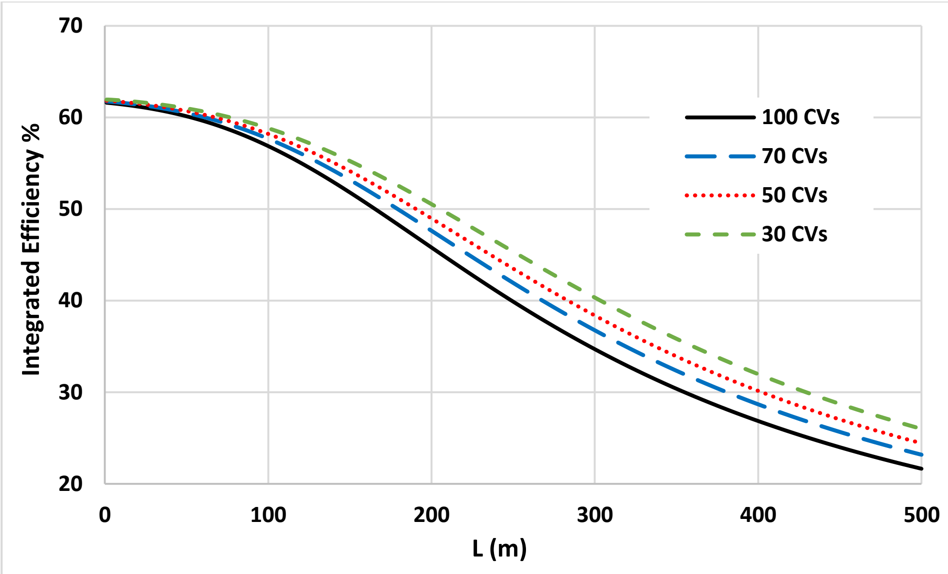

Figure 10: PTC efficiency with the cavity receiver.

Not all solar energy is successfully absorbed by the HTF, but lost. The energy lost increases at greater temperatures, since losses through radiation grow with the fourth power of temperature. At the stagnation temperature, the efficiency is approximately constant.

A major aspect of our design aims to mirror IR radiation from the internal cavity surface back onto the absorber pipe, so we will examine the effects of varying cavity wall IR reflectivity next. For this simulation, we used a cavity aperture size = 54 mm (30 CVs), we applied the IR reflectivities of 98%, 95%, and 92%.

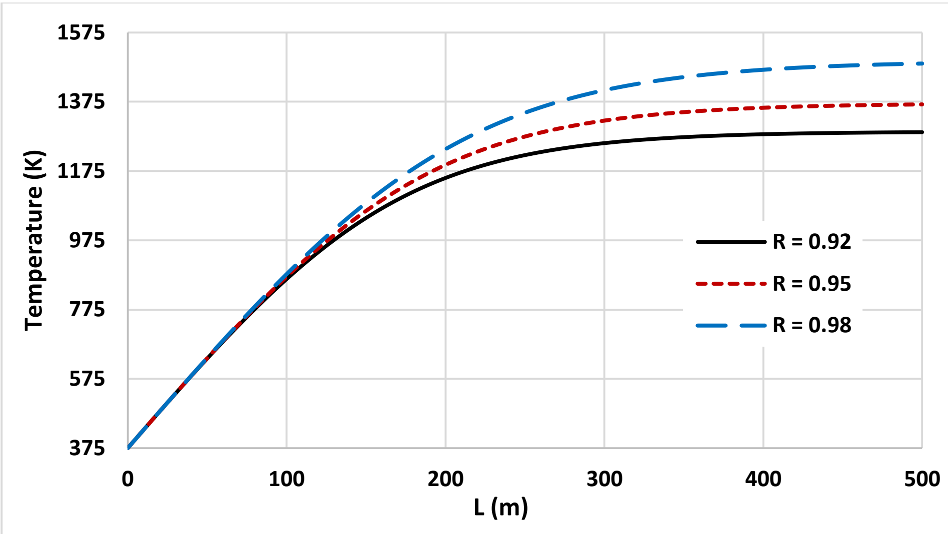

Figure 11: HTF temperature versus length L(m) of the receiver with diverse cavity IR reflectivities.

Figure 11 illustrates the influence of the cavity reflectivity (R). The performance is similar at temperatures below ~800K, but a 3% increase in the cavity wall reflectivity can result in a ~100K rise in stagnation temperature.

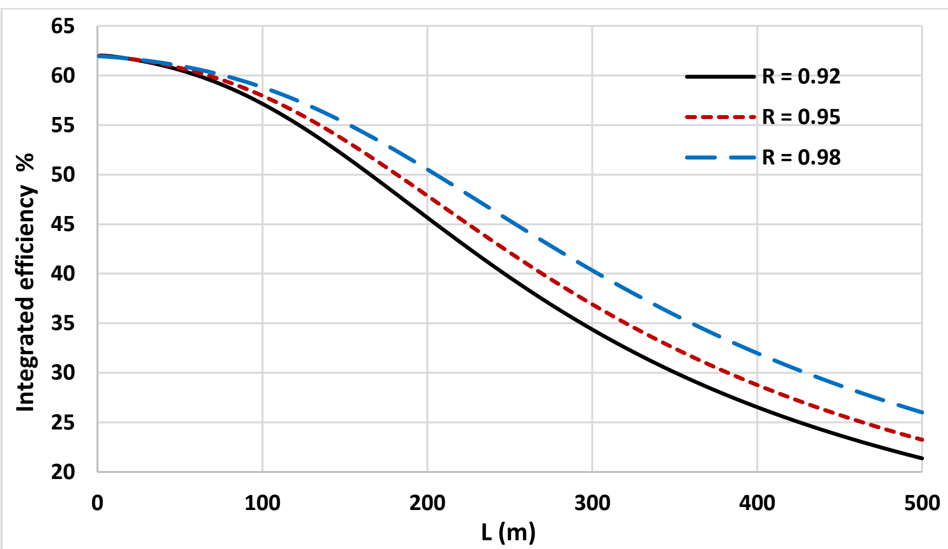

Figure 12: PTC efficiency with three cavity mirror reflectivity, as a function of length L(m).

The cavity mirror reflectivity affects the efficiency as is shown in Figure 12. Intuitively, a highly reflective cavity inner finish will absorb little radiation, and remain relatively cool.

3.2.2. Effect of aperture hot mirror coating

The cavity aperture is chiefly responsible for IR losses. We may reduce these losses through application of a HMC to the aperture glass side facing into the cavity. The effects of the HMC were simulated for a system including and excluding such a coating (denoted “W” and “WO” respectively). These simulations were performed at the cavity opening size of 54 mm and cavity mirror reflectivity R= 98%.

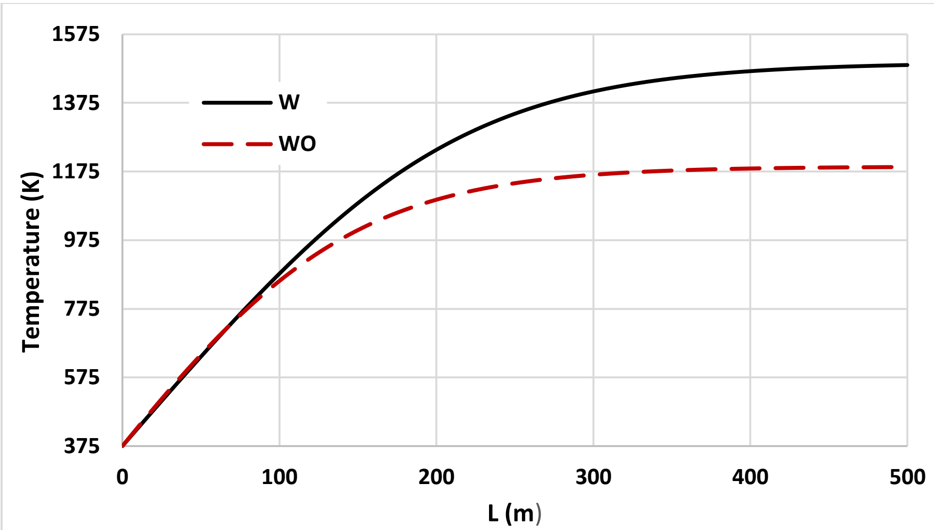

Figure 13: HTF temperature versus receiver length with and without a HMC application on the cavity opening.

Figure 13 point to the effects on the HTF temperature due to a HMC, where the coated system is capable of attaining a higher stagnation temperature. Figure 14 shows a lower efficiency for a coated cavity opening initially, up to some temperature (~650K) , but an enhanced performance afterward. We may explain this behavior this as follows: solar radiation in the IR is reflected at the aperture by the HMC before reaching the inner cavity. This adverse effect is compensated for at higher temperatures by lowered heat losses through the aperture. Figure 14 indicates that a system using one technology may not be the optimum. It would be advantageous to use a hybrid system, without hot mirror coating up to a certain length, and a hot mirror coated system after that, in order to maximize efficiency.

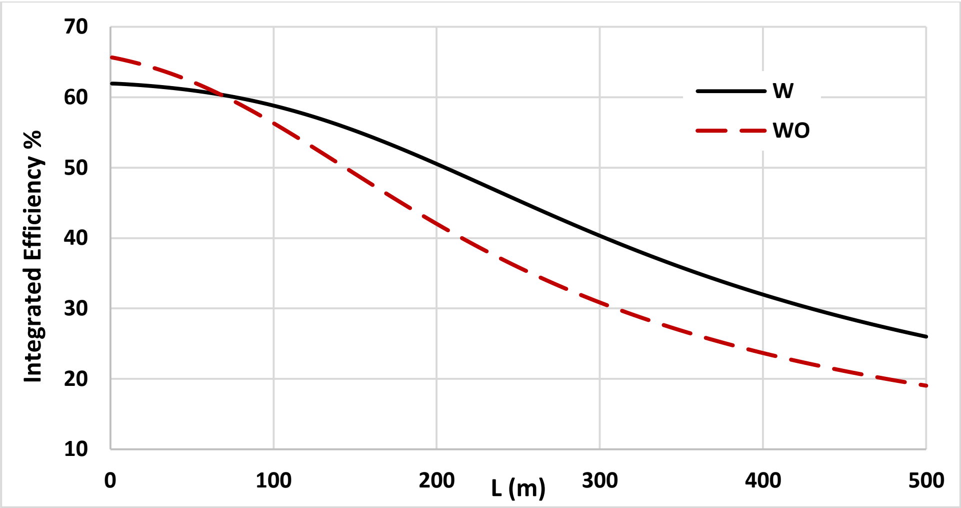

Figure 14: Efficiency with and without hot mirror coating over the aperture.

The thermal distribution profile of the outer surface of the cavity at lengths *L* (100 m and 200 m) is shown next.

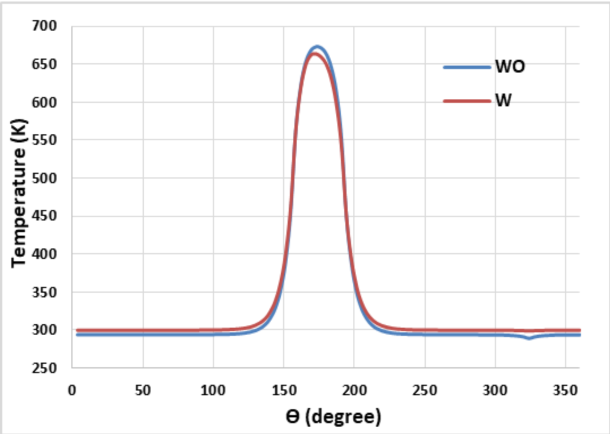

Figure 15: The temperature distribution profile of the outer surface of the cavity design L = 100 m.

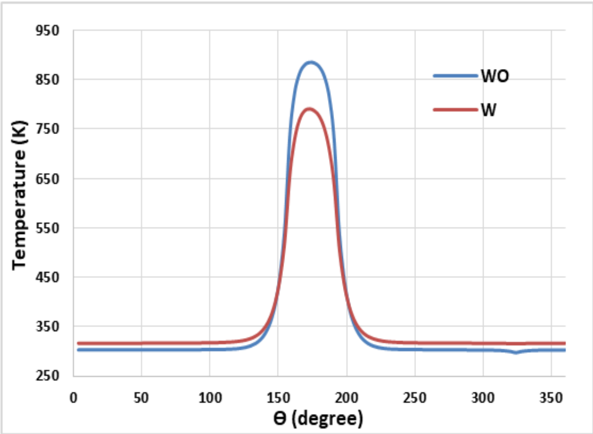

Figure 16: The temperature distribution profile of the outer surface of the cavity design at L = 200 m.

Figure 15 and Figure 16 display the outer surface temperature profile of the cavity wall perimeter without (WO) and with (W) the HMC. The angle of 0° faces towards the sun. These temperature differences can be compared to Figure 13, where the hot mirror coating becomes effective around 100 m. Most thermal losses take place at the aperture window (located between ~153° to 205°), whose temperature is greater than the metallic cavity wall. The hot mirror coating aids in reducing thermal losses, that can be observed by the ~100 K lesser window temperature at 200 m. The temperature of the metallic cavity wall is close to ambient, demonstrating reduced interaction with thermal radiation.

3.2.3. The selective coating and bare receiver

In this final section, we compare the cavity design with cavity mirror reflectivity 98%, cavity opening 30 CVs and hot mirror coating to alternatives. The alternatives are the conventional receiver with a selective coating over the absorber pipe and a bare uncoated receiver. The relevant simulation parameters that were used are mentioned in Table 2 and Table 1.

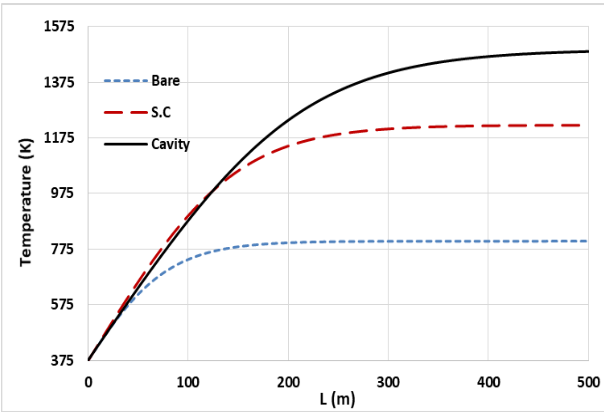

Figure 17: HTF outlet temperature at 375 K inlet temperature for differing designs.

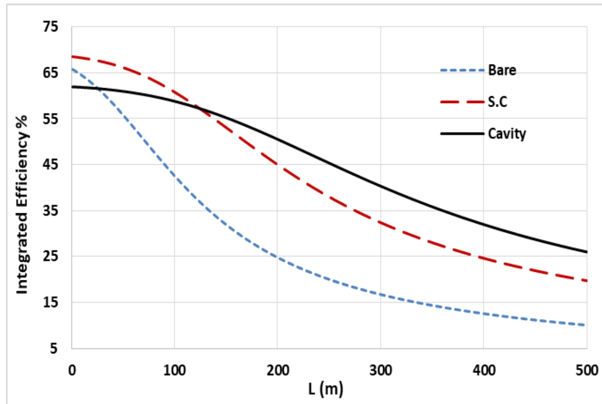

Figure 18: PTC integrated efficiency with diverse designs.

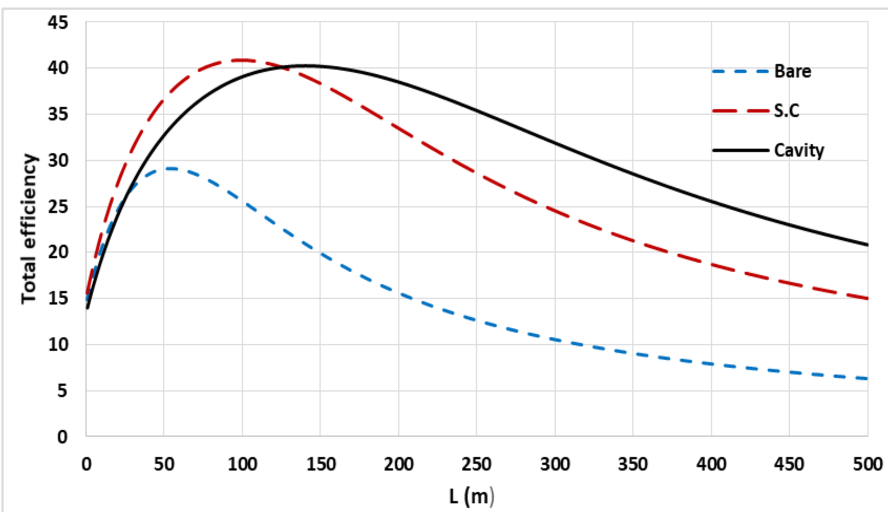

Figure 19: Total efficiency as a function of receiver length, for different designs.

Figure 17 displays the HTF temperature along the receiver length. Importantly, the selective coating on the absorber pipe will thermally decompose ~780 K, restricting its length to less than 80 m, see Figure 17. The cavity system is capable of surpassing the ceiling temperature of the selective coating. Figure 18 and Figure 19 show again total and integrated efficiency. The selective coating has a superior efficiency at lower temperatures but the higher temperature range is dominated by the cavity system.

4. Conclusion

We presented a receiver based on a cavity concept to diminish thermal radiation losses for parabolic trough solar plants and compared it to existing systems.

The experimental results from the cavity design with the application of the inner cavity IR mirror indicated a high heat retention predicted by the simulations. The Chi-squared goodness of fit comparing the simulated and experimental values, which gave p-values of 0.95 for the outer surface of the cavity and 0.8 for the absorber pipe, indicated that our model and simulation is reasonably accurate. In fact, the simulation underrated the IR mirror thermal performance at higher temperatures.

The cavity design performs very well at higher temperatures and it theoretically capable of reaching 1400 K, but this must be demonstrated first. A high operating temperature could increase the overall (Rankine) efficiency of the entire plant.

A simulated parameter was the cavity openings size, which increased efficiency with decreasing size at temperatures exceeding ~900K, as expected. However, one must incorporate the fact that a smaller aperture could lead to less concentrated light capture due to imperfect mirror optics, which would again reduce efficiency.

An increase of HM reflectivity on the aperture window increases IR retention and efficiency, especially at higher temperatures. A high IR reflectivity is important especially for larger aperture openings.

Removal of the HM entirely increases efficiency at low temperatures, since more IUR light from the sun is permitted into the receiver, but at higher temperatures efficiency from the HM system again dominates. Efficiencies can be as much as 5% higher around 800K. The aperture window temperature is very similar for a system with /without HM. The fact that different technologies perform better in different temperature regimes opens the possibility of carefully designed hybrid systems, which would perform better (economically) than each technology individually.

The cavity system is similar in efficiency to a selective coating system, if the temperature ceilings are taken into account. However, it is foreseen that a cavity type of receiver can be built cheaper, more robust, with fewer breakages and the potential of quick in situ repairs.

Acknowledgments

The authors acknowledge Materials for Energy Research Group (MERG) and Mandelstam Institute for Theoretical Research (MITP), at the University of the Witwatersrand for their kind support.

References

[1] Islam M T, Huda N, Abdullah A B and Saidur R 2018 A comprehensive review of state-of-the-art concentrating solar power (CSP) technologies: Current status and research trends *Renew. Sustain. Energy Rev.* **91** 987–1018

[2] Solar Power and Chemical Energy Systems and National Renewable Energy Laboratory (NREL) Concentrating Solar Power Projects | Concentrating Solar Power Projects

[3] Chen F, Li M, Hassanien Emam Hassanien R, Luo X, Hong Y, Feng Z, Ji M and Zhang P 2015 Study on the optical properties of triangular cavity absorber for parabolic trough solar concentrator *Int. J. Photoenergy* **2015**

[4] Ramchandra G. P, Sudhir V. P, Jyeshtharaj B. J and Vishwanath H. D Alternative designs of evacuated receiver for parabolic trough collector *Energy* **155** 66–76

[5] Antonaia A, Castaldo A, Addonizio M L and Esposito S 2010 Stability of W-Al 2 O 3 cermet based solar coating for receiver tube operating at high temperature *Sol. Energy Mater. Sol. Cells* **94** 1604–1611

[6] Kennedy C E 2002 *Review of mid-to high-temperature solar selective absorber materials* (National Renewable Energy Lab., Golden, CO.(US))

[7] Kennedy C E and Price H 2005 Progress in Development of High-Temperature Solar-Selective Coating *ASME Int. Sol. Energy Conf. Sol. Energy* 749–55

[8] Canan K 2013 Performance analysis of a novel concentrating photovoltaic combined system *Energy Convers. Manag.* **67** 186–96

[9] Miller D C, Khonkar H I, Herrero R, Antón I, Johnson D K, Hornung T, Schmid-Schirling T, Vinzant T B, Deutch S, To B, Sala G and Kurtz S R 2017 An end of service life assessment of PMMA lenses from veteran concentrator photovoltaic systems *Sol. Energy Mater. Sol. Cells* **167** 7–21

[10] Kaluba V S and Ferrer P 2016 A model for hot mirror coating on solar parabolic trough receivers *J. Renew. Sustain. Energy* **8** 053703

[11] Kaluba V S, Mohamad K and Ferrer P Experimental and simulated Performance of Heat Mirror Coatings in a Parabolic Trough Receiver *Submitt. Appl. Energy J. ArXiv190800866 Physicsapp-Ph*

[12] Mohamad K and Ferrer P 2019 Cavity receiver designs for parabolic trough collector *ArXiv190911053 Phys.*

[13] Patil R G, Panse S V and Joshi J B 2014 Optimization of non-evacuated receiver of solar collector having non-uniform temperature distribution for minimum heat loss *Energy Convers. Manag.* **85** 70–84

[14] Mohamad K and Ferrer P Experimental and numerical measurement of the thermal performance for parabolic trough solar concentrators *Proc. 63th Annu. Conf. South Afr. Inst. Phys. SAIP2018 ArXiv190800515 Physicsapp-Ph*

[15] Mohamad K and Ferrer P Computational comparison of a novel cavity absorber for parabolic trough solar concentrators *Proc. 62th Annu. Conf. South Afr. Inst. Phys. SAIP2017 ArXiv190713066 Physicsapp-Ph*

[16] Grena R 2011 Efficiency Gain of a Solar Trough Collector Due to an IR-Reflective Film on the Non-Irradiated Part of the Receiver *Int. J. Green Energy* **8** 715–33

[17] Chen F, Li M, Xu C and Wang L 2014 Study on heat loss performance of triangle cavity absorber for parabolic trough concentrators *Materials for Renewable Energy and Environment (ICMREE), 2013 International Conference on* vol 3 (IEEE) pp 683–689

[18] Xiong Y, Wu Y, Ma C, Traore M K and Zhang Y 2010 Numerical investigation of thermal performance of heat loss of parabolic trough receiver *Sci. China Technol. Sci.* **53** 444–52

[19] Chen F, Li M, Zhang P and Luo X 2015 Thermal performance of a novel linear cavity absorber for parabolic trough solar concentrator *Energy Convers. Manag.* **90** 292–299

[20] Liang H, Fan M, You S, Xia J, Zhang H and Wang Y 2018 An analysis of the heat loss and overheating protection of a cavity receiver with a novel movable cover for parabolic trough solar collectors *Energy* **158** 719–729

[21] Zhai H, Dai Y, Wu J and Wang R 2008 Study on trough receiver for linear concentrating solar collector *Proceedings of ISES World Congress 2007 (Vol. I–Vol. V)* (Springer) pp 711–715

[22] Facão J and Oliveira A C 2011 Numerical simulation of a trapezoidal cavity receiver for a linear Fresnel solar collector concentrator *Renew. Energy* **36** 90–96

[23] Mohamad K and Ferrer P 2019 Parabolic trough efficiency gain through use of a cavity absorber with a hot mirror *Appl. Energy* **238** 1250–1257

[24] Mohamad K S B *Efficiency gain of the solar trough receiver using different optically active layers* Thesis (Johanesburg, South Africa: University of the Witwatersrand)

[25] Pech A J and Soberanis M E 2012 Efficiency curves analysis of a parabolic trough solar collector in the Yucatan Peninsula *J. Renew. Sustain. Energy* **4** 021203

[26] Forristall R 2003 *Heat transfer analysis and modeling of a parabolic trough solar receiver implemented in engineering equation solver* (National Renewable Energy Lab., Golden, CO.(US))

[27] Mohamad K and Ferrer P [Patent] Thermal radiation loss reduction in a parabolic trough receiver by the application of a cavity mirror and a hot mirror coating.

[28] Dudley V E, Kolb G J, Mahoney A R, Mancini T R, Matthews C W, Sloan M and Kearney D 1994 Test results: SEGS LS-2 solar collector *Nasa Stirecon Tech. Rep. N* **96**

[29] MIRO SUN Alanod Solar Company

[30] Ferrer P 2008 Enhanced efficiency of a parabolic solar trough system through use of a secondary radiation concentrator *South Afr. J. Sci.* **104** 383–388